



Universiteit
Leiden
The Netherlands

Seeing dynamic phenomena with live scanning tunneling microscopy

Frenken, J.W.M.; Groot, I.M.N.

Citation

Frenken, J. W. M., & Groot, I. M. N. (2017). Seeing dynamic phenomena with live scanning tunneling microscopy. *Mrs Bulletin*, 42(11), 834-841. doi:10.1557/mrs.2017.239

Version: Not Applicable (or Unknown)

License: [Leiden University Non-exclusive license](#)

Downloaded from: <https://hdl.handle.net/1887/72541>

Note: To cite this publication please use the final published version (if applicable).

STM goes live: seeing dynamic phenomena with the scanning tunneling microscope

Joost W.M. Frenken^{*1} and Irene M.N. Groot²

¹ Advanced Research Center for Nanolithography, Science Park, P.O. Box 93019, 1090 BA Amsterdam, The Netherlands

² Leiden Institute of Chemistry, Leiden University, PO Box 9502, 2300 RA Leiden, The Netherlands

Scanning Tunneling Microscopy is an excellent technique to image the surfaces of materials with extreme spatial resolution. However, it is difficult to maintain its imaging quality, when applying the technique under the conditions of many practical processes, such as chemical vapor deposition and catalysis. In this review article, we describe two special classes of STM instruments that are capable of maintaining good imaging quality under ‘difficult’ conditions, namely one for high and variable temperatures and the other for the combination of high temperatures and high gas pressures. In both cases, we discuss the special design features that make these instruments robust with respect to the challenging imaging conditions and provide examples to illustrate how they are applied.

Scanning Probe Microscopy, Graphene, Chemical Vapor Deposition (CVD) (deposition), Surface Chemistry, Catalytic

Introduction

Scanning Tunneling Microscopy (STM) was introduced in the early nineteen eighties^{1,2}. The ability to ‘see’ atoms directly at the surfaces of a wide variety of materials provided the surface-science community with an enormous boost and later also became indispensable in other fields of science. Complex structures were recognized easily, which greatly helped solving the geometrical puzzles of several surface reconstructions^{2,3}. The STM images also provided the first realistic views of the defects that often dominate the behavior of surfaces. Where ideal, flat surfaces had dominated the description of surfaces thus far, STM

made it impossible to ignore the ‘omnipresence’ of steps⁴. In addition, also point defects, such as vacancies, adatoms and kinks became familiar elements. In many practical processes in which surfaces play an essential role, this role can be traced back to these defects. Think of crystal growth, where a new layer on a crystal may nucleate by the clustering of newly arriving adatoms and further growth of that cluster proceeds via addition of adatoms to the perimeter, i.e. to a step⁵. Think of the sintering between two pieces of solid, which involves diffusion of many atoms, each of which has to liberate itself from a kink site and to subsequently move either along a step or over a terrace before it becomes incorporated in the region where the solids meet⁶. And think of heterogeneous catalysis, where steps and other defects establish chemically distinct sites with altered and often enhanced interaction with adsorbed molecules; in many cases, these are considered to be the ‘active’ sites for a chemical reaction⁷.

Early STM images immediately fueled the dream that this technique would make it possible to follow some of these processes dynamically and reveal in detail where and how they take place and what structural features at the surface they involve. Obviously, this would necessitate making the STM observations under the conditions under which these processes take place. Technically, this turned out to be far from trivial, as STM is a delicate measuring technique that is ‘vulnerable’ to many external influences. These can make STM imaging challenging or even practically impossible. In this review, we concentrate on two of these challenges, namely those introduced by high and even varying temperatures and those involved in high gas pressures (and flows), as well as their combination. We describe the instruments that we have developed to face these challenges and illustrate their application with two examples, namely the growth of graphene by low-pressure Chemical Vapor Deposition (CVD) and the surface structure of catalysts under operation conditions.

Variable-temperature STM

Thermal drift

Early STM setups were designed for imaging at room temperature. Nevertheless, a common problem was that even minor temperature variations in

the laboratory or the last few degrees of cooling down of the specimens after a high-temperature preparation step, would lead to a noticeable, continuous translation of the STM tip with respect to the imaged surface, both parallel to the surface and perpendicular⁸. This drift results from the differences in thermal expansion between the components in the mechanical path between the surface of the specimen and the tip, including the tip and the specimen itself. Thermal drift distorts the images, makes it difficult to repeat observations on the same area and even leads to situations where the tip-surface distance drifts out of the limited control range of the instrument; in the latter case, either the tip can no longer be brought into tunneling range with respect to the surface or the tip cannot be retracted sufficiently and is jammed into the surface.

As a consequence of this sensitivity to temperature, it has taken relatively long before the first STM instruments were developed that targeted other temperatures than room temperature. Low-temperature STM setups establish a class of their own⁹. Since most expansion coefficients reduce to practically zero at cryogenic temperatures, these instruments exhibit spectacularly low thermal drift. Another advantage of low temperatures is that they make the step in the occupation number of electronic states extremely sharp, which is exploited in sensitive spectroscopy¹⁰. For the study of dynamic processes, cryogenic temperatures are usually not attractive, since thermally activated processes slow down dramatically, to practically zero, as the temperature is lowered.

At high temperatures, thermal drift rapidly becomes a serious issue and in the next section we will describe how this has been dealt with successfully.

Design features of a (truly) variable-temperature STM setup

As explained, the thermal drift observed in STM images results from the differences in the thermal expansion (or contraction) of all elements in the mechanical path between tip and surface. The simplest way to make this difference negligible at arbitrary sample temperatures would be to bring all these mechanical elements, including the specimen, to the same temperature, for example by putting the instrument in an oven. When one designs it such that the mechanical path contains two parts with identical materials that compensate each

other's expansions and contractions exactly, there should be no thermal drift, in principle. This approach is typical for cryogenic STM setups and it has been adopted in a small number of high-temperature STMs¹¹. The most important problem with it is that the piezoelectric elements that are typically employed to actuate the STM tip, cannot be used above a certain temperature, the Curie temperature, at which the piezo element spontaneously depolarizes¹². For a material such as PZT (lead zirconate titanate), the limiting temperature is 350°C or even lower and already at much lower temperatures, the polarization degrades noticeably. In order to avoid this, it is essential to keep the temperature of the piezo elements low, even when the tip scans over a hot specimen surface. This brings in the additional challenge to tailor the temperature profile over the STM setup, such that while the specimen is hot, the piezo element remains relatively cool. Again, the condition is that the combination of all expansions leads to no more than a small displacement of the tip with respect to the surface. On top of this we require that the expansions should cancel each other not only after completion of a change in temperature, but also *during* temperature changes. Otherwise, it would become very impractical to perform a series of measurements at different temperatures, since the typical temperature settling time in such an instrument can be several hours. This extra requirement implies that the characteristic timescales for temperature changes should be matched between those components that are supposed to compensate each other's expansions.

This may seem an unrealistic combination of requirements, certainly if they should be met for specimens of different materials, each with a different expansion coefficient. Nevertheless, we have succeeded in constructing a Truly Variable-Temperature Scanning Tunneling Microscope that can image a surface while it is heated from room temperature to e.g. 1300 K and that can keep a certain area on the surface in view over a temperature window of approximately 300 K¹³. The instrument has a modular design, in which the specimen plus its holder, the scanner, and the support table that carries the two, each exhibit the required internal match of expansions and timescales (see **Figure 1**).

This modularity requires a peculiar geometry, in which for example the height of the sample is fixed inside the sample holder by pushing it with a spring with its surface against ridges in the holder (see **Figure 2**).

In this way, the thickness and expansion coefficient of the specimen itself, the hottest element during high-temperature operation, have no effect on the tip-sample distance. This simple design choice eliminates much of the drift in the corresponding z-direction. Next to a well-chosen geometry, an extensive numerical analysis was required in order to quantitatively predict the thermal behavior in full detail, e.g. to calculate the time-dependent temperature of each component following a change in the heating power supplied to the specimen. Parameters that could be adjusted in this exercise were the precise dimensions of all components and, within certain restrictions also the materials¹⁴. This optimization has resulted in a sample holder with a delicate geometry (**Figure 2**) in combination with a scanner with a relatively simple design (**Figure 1**). Sample and tip need to be mounted accurately (0.1 mm) in order to ensure the desired degree of compensation of expansions along the z-direction.

Figure 3 shows a photograph of the Truly Variable-Temperature Scanning Tunneling Microscope, complete with spring suspension and eddy current damping¹³. Using a wobble stick and a simple transport system, one can conveniently exchange both the sample and the scanner to separate UHV chambers, one of which serves as a storage chamber and another as a load-lock system.

Special attention has been given to the control electronics and software of this instrument, in order to enable high-speed observations of fast phenomena, such as surface diffusion, phase transitions and growth processes. The mechanical resonances of the instrument allow us to routinely image at rates of several frames/sec on surfaces that are not too rough. With a special scanner, optimized for high resonance frequencies, we have demonstrated imaging rates beyond 100 frames/sec.

Live observations of graphene growth at high temperatures

The high-temperature capabilities of our Truly Variable-Temperature Scanning Tunneling Microscope are illustrated in a series of experiments in which we investigated the growth of single-layer graphene by low-pressure Chemical Vapor Deposition (CVD) on transition metal surfaces. **Figure 4** shows two STM images in which the growth of graphene was followed on a Rh(111) surface¹⁶⁻¹⁸. Prior to these two images, the experiment started with a seeding procedure, in which the Rh surface was exposed at room temperature to 4×10^{-7} mbar s of ethylene gas (C_2H_4), which was enough to saturate the surface with a disordered molecular overlayer. While the surface was imaged continuously, it was heated up at a rate of 0.2 K/s. This led to rearrangements in the overlayer, in which the molecules lost their hydrogen and initially formed small carbon clusters. At 808 K, the first low-quality moiré patterns were observed that indicated the formation of small graphene patches. Like on most substrates, there is a lattice mismatch between graphene and the rhodium substrate, which generates a modulation in the height of the graphene: a moiré pattern. Twelve lattice units of graphene are a close match to thirteen lattice units of rhodium. We use these patterns as ‘detectors’ of the presence of graphene and as indicators of the quality of the graphene. Panel (A) of **Figure 4** shows the situation at 975 K. The drift in the z-direction between room temperature and 975 K was sufficiently low (~ 100 nm) that no coarse height adjustments were needed at all over this entire temperature range. At this temperature, the rhodium surface was covered by a modest density of medium-size single-layer graphene patches. Within each patch, typically a few graphene orientations can be recognized from the differences in orientations and lattice constants of the moiré patterns. Between panels (A) and (B), we exposed the surface during a period of 76 min at a constant temperature of 975 K to further ethylene at pressures ranging from 3×10^{-9} to 1×10^{-8} mbar. The final result is shown in panel (B). We recognize that the entire surface is covered with a single monolayer of graphene. The patchwork of different orientations results directly from the variation in initial orientations with which the individual patches were nucleating in the seeding procedure that led to the configuration in panel (A). The graphene completely overgrows the atomic step on the rhodium substrate. The

only two regions in panel (B) that are different, are the so-called Rh double-layer defects, indicated by the two arrows. These are regions where diffusing rhodium adatoms on a terrace of bare rhodium were encircled by graphene; when further graphene growth reduced the bare rhodium area, the areal density of the rhodium adatoms grew until it reached a level that was high enough to nucleate a new rhodium monolayer. We observed that this process would typically lead to structures that were two rhodium layers high, rather than one.

In addition to heating and high-temperature exposure experiments, we also performed cooling experiments in the absence of ethylene¹⁷. For entropic reasons, a lowering of the temperature leads to a reduction of the bulk solubility of carbon atoms in the rhodium substrate, which results in segregation of dissolved carbon, back to the surface. Therefore, when we cooled the rhodium surface after it was covered at high temperature by a full graphene monolayer, we obtained a rough graphene layer at room temperature, which we ascribe to accumulation of segregated carbon below the graphene. When we followed the same procedure, starting at high temperature with an incomplete graphene layer, we observed further growth of the graphene due to incorporation of segregated carbon at the graphene edges. This is illustrated in **Figure 5**. Again, we take advantage of the low-drift properties of the microscope, by imaging a single region at the surface not only at high temperatures but also over a range in temperature.

ReactorSTM

Catalysis

One of the primary motivations for detailed investigations of clean and adsorbate-covered metal surfaces has always been the role that these surfaces and their adsorption processes are thought to play in heterogeneous catalysis⁷. Often, the metal in a catalyst is present in the form of nanoparticles on a convenient support. Traditionally, the idea is that the catalytic metal surface presents favorable adsorption sites that interact significantly with the adsorbed (reactant) molecules and affect their internal bonding as well as the pathways and activation energies for their chemical conversion. On the other hand, the interaction cannot be too strong, because this would make it too difficult for molecules, in particular

product molecules, to desorb. What is left out from this description, is the possibility for the metal to engage intimately in chemical intermediates with the reactant molecules. In other words, the catalyst may be involved actively in intermediate products and thus introduce altogether new reaction pathways. Alternatively, the modifications may lead to an alternative form of the catalyst that may exhibit a higher activity or selectivity for the desired chemical reaction than the bare metal surface. Even in cases where the formation energies of such intermediate products or modified forms of the catalyst would be unfavorable, the *free energy* for their formation could still be favorable under the high pressures that are typically applied in industrial catalysis. There is a growing body of evidence that such situations establish the ‘rule’ rather than the exception.

When catalysts indeed acquire their active forms only under reaction conditions, it is essential that we investigate them under these conditions, typically under high reactant pressures and at elevated or even high temperatures. This insight has fueled the recent adaptation of an expanding range of sensitive surface-science techniques that are traditionally restricted to ultrahigh vacuum conditions and low rather than high temperatures, towards the more daring conditions of practical catalysis¹⁹. Among these are STM, Surface X-Ray Diffraction, X-Ray Photoelectron Spectroscopy and Transmission Electron Microscopy. Here, we introduce the special design features of the high-pressure, high-temperature STM setup that we refer to as the ReactorSTM²⁰.

Design of a high-pressure high-temperature STM setup

Three independent considerations have forced us to adopt a highly unconventional design for the ReactorSTM, our Scanning Tunneling Microscope for high pressures and high temperatures²⁰. (i) In order to be able to perform our experiments on well-defined, e.g. (initially) clean and well-ordered single-crystal surfaces, the setup needs to contain regular preparation and characterization tools and ultrahigh vacuum. (ii) During the high-pressure experiments, also with highly corrosive gases, ideally only the model catalyst should be exposed to the gases, while the delicate components of the setup, such as the piezo element and the sample heating device as well as all other surface-science tools, should be kept in

(ultrahigh) vacuum. (iii) For rapid variations in the composition of the reactant gas mixture and for sensitive and fast measurements of the catalytic activity, the total gas volume should be minimized. The setup is designed as the combination of a traditional ultrahigh vacuum system with a tiny high-pressure gas cell that is integrated with the STM (see **Figure 6**).

The sample is carried by a convenient sample holder with heating and temperature measurement integrated. A transport system makes it easy to introduce new samples into the system and to bring samples to separate vacuum chambers (see **Figure 7**) for sputter cleaning, various forms of deposition, Low-Energy Electron Diffraction, Auger Electron Spectroscopy, X-Ray Photoelectron Spectroscopy (not shown in **Figure 7**) and Scanning Tunneling Microscopy. When the sample is in the STM-position, a Kalrez seal is located between the surface of the sample and the reactor body (see **Figure 6**). Between the reactor and the piezo element of the STM is a Viton seal. Together, the two seals make it possible to fill up the tiny reactor volume with gas mixtures up to a total pressure of 6 bar, while the pressure in the surrounding ultrahigh vacuum chamber remains unaffected. Presently, the setup is being modified to accommodate pressures up to 20 bar. The only STM components that are exposed to the gases are the tip and its gold-coated holder, which can slide in sub-micrometer steps in order to provide coarse z-positioning, bringing the surface into the z-control range of the piezo element. The piezo element itself is kept in vacuum. The reactor is usually operated in flow mode and the gases are led into and out of the small reactor volume via capillaries. These capillary gas lines are thin enough that they are easily integrated with a traditional spring suspension and eddy current damping system that decouples the system mechanically from external vibrations.

Live observations of the structure of an oxidation catalyst in action

Here, we illustrate the successful application of the ReactorSTM with two examples of special structures that form spontaneously at model catalyst surfaces under realistic reaction conditions. In the first example, we concentrate on the close-packed Pt(111) surface²¹. Platinum is known to be an excellent oxidation catalyst and it is one of the dominant materials in the three-way car catalyst. Even

though this has fueled an impressive number of detailed studies of the structure of platinum surfaces, their interaction with oxygen and other adsorbates, and the interaction between various molecules on platinum, only a small number of these have directly addressed the atomic-scale structures under actual reaction conditions.

In early, high-pressure STM studies^{22,23} and accompanying Surface X-Ray Diffraction experiments on Pt(110) under CO oxidation conditions²⁴, we found evidence for the formation of an ultrathin oxidic layer on the metal surface and we argued that this surface oxide would serve as the intermediate product in a Mars-Van-Krevelen-type reaction mechanism. Whether this oxidized surface should be regarded as the active state of the catalyst and whether this behavior can be generalized further to other oxidation catalysts and even to other reaction systems, forms the subject area of an ongoing debate. What is clear, is that there is a delicate interplay between the chemical environment in which the catalyst is placed, the structure of the catalyst and the resulting catalytic activity, and that this interplay can be unraveled only by high-resolution observations of the catalyst structure and performance while it is fully exposed to the reactants at the appropriate combination of partial pressures and temperature. Panels (a) – (d) of **Figure 8** show some of the first atomically resolved STM images that we have obtained with the ReactorSTM of a platinum surface, Pt(111), at a high temperature and a high pressure of oxygen²¹. The observed structure is a spoked-wheel pattern of raised atoms.

We have used additional STM-observations under a variety of conditions and a detailed inspection of X-Ray Photoelectron spectra and compared our results to earlier observations under various oxidative conditions to verify that this structure corresponds to the geometry shown in panel (e) of **Figure 8**. Each spoke is an oxidized row of seven platinum atoms, each accompanied by four oxygen atoms. The oxide rows are embedded in the first layer of the platinum surface, where each takes the place of eight ‘regular’ platinum atoms. The red dots between the spokes form a p(1×2)-O chemisorption structure. Similar structural elements are also present in some lower-pressure observations on

Pt(111) under the influence of more strongly oxidizing species, such as NO₂, but the density of oxide rows is much lower in those cases. We speculate that by raising the chemical potential of oxygen via the high partial pressure of O₂ in our observations, we have counter-acted the high surface stress that is involved in the spoked-wheel structure and thus brought this surface into a state where it is much more prone to donate oxygen atoms to other oxidation reactions. In other words, by stabilizing an energetically unfavorable reaction intermediate, the high O₂ pressure may be enabling a new oxidation pathway.

Live observations of the accumulation of a reaction product

For our final example, we turn to the Fischer-Tropsch (FT) synthesis reaction²⁵. Like oxidation catalysis, FT synthesis has a rich history; it is the reaction that is used to form linear alkane and alkene chains from CO and H₂, for example to produce synthetic fuel. Catalysts for this reaction are often based on cobalt and the mechanism is usually thought to be a straightforward, stepwise addition of alkyl (CH₂) units to one end of a linearly growing hydrocarbon chain²⁶. With a fixed probability per unit for this process to terminate, the resulting product distribution takes on a simple, exponential form, as is indeed found in practice.

As **Figure 9** illustrates, our high-pressure, high-temperature STM observations show the formation of an ordered overlayer on the Co(0001) model catalyst surface²⁷. The STM image was taken 40 min after we had started the exposure of the cobalt surface, stabilized in an H₂:Ar = 1:4 mixture at 4 bar and ~495 K for 2 hours, to so-called syngas, a stoichiometric 1:2 mixture of CO and H₂. Earlier STM images had revealed the nucleation and growth of overlayer islands and the image in **Figure 9** shows the final configuration, obtained when the overlayer had colonized the entire surface. Stripe-like patterns, such as those in the STM image, are familiar in the context of the adsorption and spontaneous ordering of linear hydrocarbon molecules on metal surfaces²⁸ and this interpretation is illustrated schematically in panels (c) and (d). Nevertheless, two aspects of the pattern are surprising. The presence of a regular stripe pattern with a well-defined period indicates that the surface is populated primarily with a

single chain length, even though the exponential distribution of chain lengths, mentioned above, should be rather wide. Also surprising is that the observed, average stripe width of 1.8 ± 0.3 nm corresponds to chains with a remarkable length of 14 ± 2 carbon atoms, much larger than the average chain length expected from a simple, unpromoted cobalt catalyst. We explain these observations in terms of two competing effects. Even though the shorter molecules are formed much more abundantly than the long ones, they readily desorb from the metal surface; hence, their surface coverage is established almost instantaneously, but it is negligibly low. It takes much more time for a significant number of long molecules to form, but since they have more interaction with the substrate, they will eventually accumulate to higher concentrations. A simple, numerical calculation shows that the first molecular length for which this accumulation will lead to a concentration at which islands should be expected to form, is in the order of 15 C atoms and that the time required for this accumulation to take place under the conditions of our experiment is in the order of 20 min. Both estimates correspond well with the experimental observations and provide confidence in this interpretation²⁷.

The scenario revealed here, implies that in the early stages of the ‘life’ of the catalyst, the reaction itself is modifying the catalyst, in this case not by restructuring the metal surface, as we found for Pt(111), but by covering the metal surface with a chemically nearly inert film. The mere presence of this film should reduce the attraction between the substrate and newly formed hydrocarbon molecules on top. We imagine that this makes it easier for the chain-growth process of these new molecules to terminate and for the molecules to desorb. This will significantly reduce the average chain length, produced in the process, which should be regarded as a reduction in the performance of the catalyst. On the other hand, the easier release of the product molecules may be a highly necessary property of the catalyst in order to avoid its direct inactivation by a rapidly thickening, tightly bound product film. Maybe, the product monolayer that we have identified here is therefore somewhat of a ‘mixed blessing’.

Summary and outlook

In this review, we have described two STM systems for the observation of *live* processes under realistic process conditions, the Truly Variable Temperature Scanning Tunneling Microscope and the ReactorSTM, and we have provided a few examples of research conducted with these instruments. These STM developments go hand in hand with similar developments in Atomic Force Microscopy²⁹ and in a growing number of other experimental techniques that were originally thought to be strictly limited to the conditions of ultrahigh vacuum and room temperature (or cryogenic temperatures). Technically, this often involves serious complications in the design and construction of these instruments and this makes the effort required for these developments significant. This is why we regard it essential that the resulting instruments are professionalized and commercialized, so that the entire research community can benefit from them.

Acknowledgments

This article is dedicated to our ‘pioneers’ for the two featured STM-systems, Kobus Kuipers, Peter Rasmussen and Bas Hendriksen. Over a period of more than two decades, their work has been supported, augmented and brought to further fruition by an ‘army’ of scientific and technical staff members at Leiden University and, before that, at AMOLF in Amsterdam, that is too large to do proper justice to by mentioning all of them individually. Finally, we are indebted to Gertjan van Baarle and his crew at Leiden Probe Microscopy B.V. for teaming up with us in these endeavors and turning our prototypes into real products.

References

1. G. Binnig, H. Rohrer, Ch. Gerber, E. Weibel, *Phys. Rev. Lett.* **49** 57 (1982).
2. G. Binnig, H. Rohrer, Ch. Gerber, E. Weibel, *Phys. Rev. Lett.* **50** 120 (1983).
3. K. Takayanagi, Y. Tnishiro, S. Takahashi, M. Takahashi, *Surf. Sci.* **164** 367 (1985).
4. B.S. Swartzentruber, Y-W. Mo, R. Kariotis, M.G. Lagally, M.B. Webb, *Phys. Rev. Lett.* **65** 1913 (1990).

5. A. Pimpinelli, J. Villain, *Physics of Crystal Growth* (Cambridge University Press, Cambridge, UK, 1998).
6. S.-J.L. Kang, *Sintering: Densification, Grain Growth & Microstructure* (Elsevier Butterworth-Heinemann, Oxford, UK, 2005).
7. G.A.Somorjai, Y. Li, *Introduction to Surface Chemistry and Catalysis, 2nd Edition* (John Wiley & Sons, Hoboken, NJ, USA, 2010).
8. P. Rahe, R. Bechstein, A. Kühnle, *J. Vac. Sci. Technol. B* **28** C4E31 (2010).
9. A.M.J. den Haan, G.H.C.J. Wijts, F. Galli, O. Usenko, G.J.C. van Baarle, D.J. van der Zalm, T.H. Oosterkamp, *Rev. Sci. Technol.* **85** 035112 (2014).
10. Y.J. Song, A.F. Otte, Y. Kuk, Y. Hu, D.B. Torrance, P.N. First, W.A. de Heer, H. Min, S. Adam, M.D. Stiles, A.H. MacDonald, J.A. Stroscio, *Nature* **467** 185 (2010).
11. J.W. Lyding, S. Skala, J.S. Hubacek, R. Brockenbrough, G. Gammie, *J. Micr.* **152** 371 (1988).
12. A.J. Moulson, J.M. Herbert, *Electroceramics: Materials, Properties, Applications* (John Wiley & Sons, Chichester, UK, 2003).
13. M.S. Hoogeman, D. Glastra van Loon, R.W.M. Loos, H.G. Ficke, E. de Haas, J.J. van der Linden, H. Zeijlemaker, L. Kuipers, M.F. Chang, M.A.J. Klik, J.W.M. Frenken, *Rev. Sci. Instrum.* **69** 2072 (1998).
14. L. Kuipers, R.W.M. Loos, H. Neerings, J. ter Horst, G.J. Ruwiel, A.P. de Jongh, J.W.M. Frenken, *Rev. Sci. Instr.* **66** 4557 (1995).
15. Leiden Probe Microscopy B.V., J.H. Oortweg 19, 2333 CH Leiden, The Netherlands, www.leidenprobemicroscopy.com
16. G.C. Dong, D.W. van Baarle, M.J. Rost and J.W.M. Frenken, *ACS Nano* **7** 7028 (2013).
17. G.C. Dong, D.W. van Baarle and J.W.M. Frenken, in *Advances in Graphene Science*, M. Aliofkhazraei, Ed. (InTech, 2013) p. 33.
18. G.C. Dong, D.W. van Baarle, M.J. Rost, J.W.M. Frenken, *N. J. Phys.* **14** 053033 (2012).
19. *Operando studies in heterogeneous catalysis*, I.M.N. Groot and J.W.M. Frenken, Eds. (Springer-Verlag, Berlin, Germany, 2017)
20. C.T. Herbschleb, P.C. van der Tuijn, S. Roobol, V. Navarro-Paredes, J.W. Bakker, Q. Liu, D. Stoltz, M.E. Cañas-Ventura, G. Verdoes, M. van Spronsen, M.

Bergman, L. Crama, I. Taminiau, A. Ofitserov, G.J. van Baarle, J.W.M. Frenken, *Rev. Sci. Instrum.* **85** 083703 (2014).

21. M.A. van Spronsen, J.W.M. Frenken, I.M.N. Groot, *Nat. Commun.* **will appear on 5 September and is still under embargo** (2017).

22. B.L.M. Hendriksen, J.W.M. Frenken, *Phys. Rev. Lett.* **89** 046101 (2002).

23. B.L.M. Hendriksen, M.D. Ackermann, S.C. Bobaru, I. Popa, S. Ferrer, J.W.M. Frenken, *Nat. Chem.* **2** 730 (2010).

24. M.D. Ackermann, T.M. Pedersen, B.L.M. Hendriksen, O. Robach, S. Bobaru, I. Popa, C. Quiros, H. Kim, B. Hammer, S. Ferrer, J.W.M. Frenken, *Phys. Rev. Lett.* **95** 255505 (2005).

25. J.J.C. Geerlings, J.H. Wilson, G.J. Kramer, H.P.C.E. Kuipers, A. Hoek, H.M. Huisman, *Appl. Cat. A: General* **186** 27 (1999).

26. G.P. Van der Laan, A.A.C.M. Beenackers, *Catal. Rev. Sci. Eng.* **41** 255 (1999).

27. V. Navarro, M.A. van Spronsen, J.W.M. Frenken, *Nat. Chem.* **8** 929 (2016).

28. K. Uosaki, R. Yamada, *J. Am. Chem. Soc.* **121** 4090 (1999).

29. S.B. Roobol, M.E. Cañas-Ventura, M. Bergman, M.A. van Spronsen, W.G. Onderwaater, P.C. van der Tuijn, R. Koehler, A. Ofitserov, G.J.C. van Baarle, J.W.M. Frenken, *Rev. Sci. Instrum.* **86** 033706 (2015).

Figure Captions

Figure 1. Schematic cross section of the Truly Variable-Temperature Scanning Tunneling Microscope. The scanner **A** is cylindrically symmetric around the axis through the tip **F**. It rests with three legs on the support block **H**. A radiation shield **E** protects the piezo element **B** against thermal radiation from the sample **C**. The sample holder **D** is clamped down against two supports by leaf springs **G**. The sample is clamped up against two ledges of the sample holder. (after ref. 13)

Figure 2. Schematic top (a) and perspective (b) views of the sample holder body. Four arms extend from the holder. Two of these, **B**, are rotated against vertical posts **A** that form part of the support block (**Figure 1**). The other two are shaped as knife edges, **E**, and are pressed down against two flat supports by two leaf springs, **C**. When the holder is heated, it expands outwards along the four extensions, but the center, **D**, stays at its original position. To enable a coarse approach, the STM tip is mounted 1 mm away from the rotation axis, **F**, around which the sample holder can be rotated with the help of an inertial piezo motor. (after ref. 13)

Figure 3. Photograph of the Truly Variable-Temperature Scanning Tunneling Microscope, complete with spring suspension and eddy current damping on a conflat flange. (courtesy of Leiden Probe Microscopy B.V.¹⁵)

Figure 4. Figure 4. STM images of graphene formation on Rh(111), starting with a seeded surface. (A) The graphene-seeded Rh surface, obtained by annealing the rhodium surface to 975 K, after exposing it to ethylene at room temperature. (B) Graphene-covered surface, after further ethylene deposition at 975K. Notice the two Rh double-layer defects, indicated by the arrows. The inset in (B) shows the superstructure spots around a first-order LEED spot of the Rh substrate. Both STM images have a size of 160 nm × 160 nm. (from ref. 17)

Figure 5. Graphene formation by segregation of dissolved carbon. (A) STM images of the same area during the cooling down of Rh(111), partly covered by graphene, after the room-temperature seeding procedure and ethylene exposure at 977K. The central rhodium terrace is at the same level as the surrounding graphene, implying that rhodium atoms are diffusing out of this area as the graphene grows. Image size: 100 nm × 100 nm. (B) Ball model illustrating the growth of graphene through segregated carbon and the corresponding reduction of Rh area. (after ref. 17)

Figure 6. Schematic cross section of the central components of the ReactorSTM. The (yellow) sample is held in a sample holder (top part) with a heater, thermocouple and electrical connections. Here, the sample is placed on top of the STM scanner part of the system. In this position, it forms the 'lid' of the 500 μl reactor. The reactor body is made of Zerodur glass. The reactants enter via a capillary from the left (blue) and the reacted gas mixture leaves the reactor through a capillary on the right (red), where it is connected to a separate Mass Spectrometry system. The small reactor is sealed off against the sample surface via a Kalrez seal and against the top of the piezo element with a Viton seal. The piezo element itself remains in ultrahigh vacuum. (from ref. 20)

Figure 7. Photograph of the complete ReactorSTM system. (courtesy of Leiden Probe Microscopy B.V.¹⁵)

Figure 8. STM observations of Pt(111) in 1 bar O₂ at 529 K. A spoked-wheel motif with embedded PtO₂ rows can be recognized, with a variety of structural defects. Panels (a)-(c) show larger domains of this structure; the star serves as a reference point and indicates slow thermal drift. The enlarged detail in panel (d) shows the atomic resolution within the spokes. Panel (e) is the ball model with the oxidized Pt atoms in light blue, the O atoms in red and the regular Pt surface atoms in dark blue (layer 1), grey (layer 2) and black (layer 3). (from ref. 21)

Figure 9. STM image of the Co(0001) surface, 40 min after the start of its exposure to 4 bar of an 1:2:2 mixture of CO, H₂ and Ar at a temperature of 483 K. The schematic pictures on the right illustrate how the overlayer forms as rows of well-organized hydrocarbon molecules. (after ref. 27)

Figures with Figure Captions

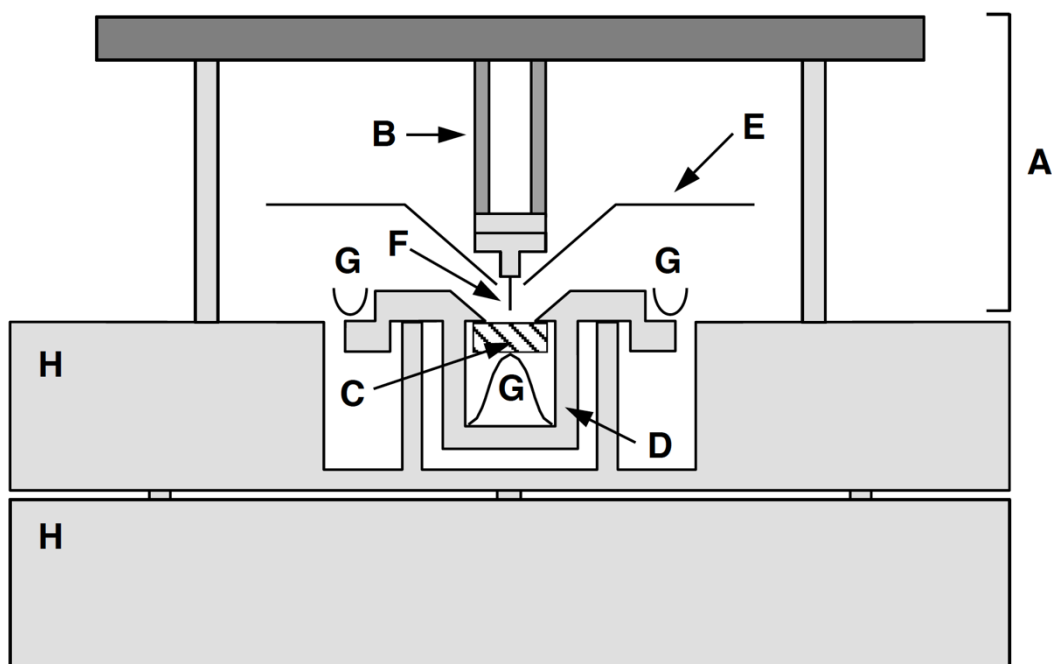


Figure 1. Schematic cross section of the Truly Variable-Temperature Scanning Tunneling Microscope. The scanner **A** is cylindrically symmetric around the axis through the tip **F**. It rests with three legs on the support block **H**. A radiation shield **E** protects the piezo element **B** against thermal radiation from the sample **C**. The sample holder **D** is clamped down against two supports by leaf springs **G**. The sample is clamped up against two ledges of the sample holder. (after ref. 13)

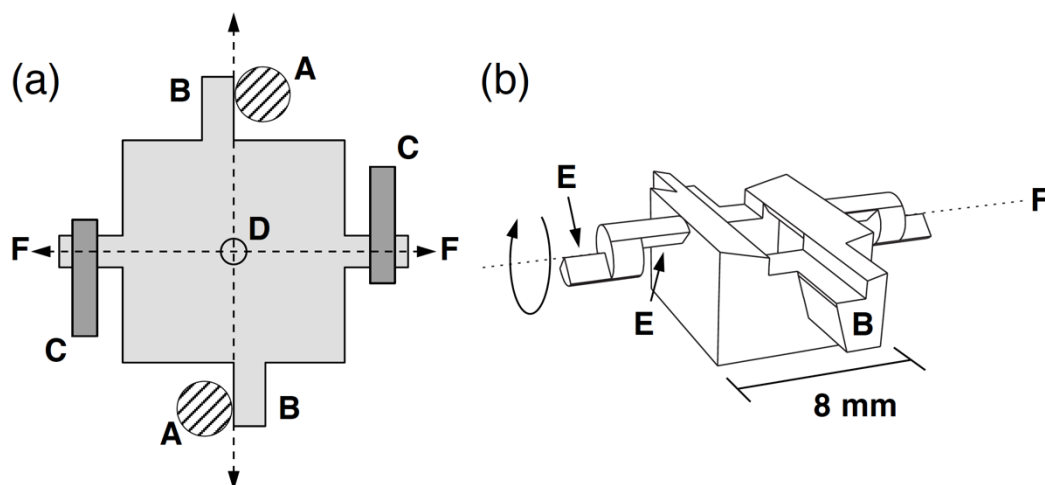


Figure 2. Schematic top (a) and perspective (b) views of the sample holder body. Four arms extend from the holder. Two of these, **B**, are rotated against vertical posts **A** that form part of the support block (**Figure 1**). The other two are shaped as knife edges, **E**, and are pressed down against two flat supports by two leaf springs, **C**. When the holder is heated, it expands outwards along the four extensions, but the center, **D**, stays at its original position. To enable a coarse approach, the STM tip is mounted 1 mm away from the rotation axis, **F**, around

which the sample holder can be rotated with the help of an inertial piezo motor. (after ref. 13)

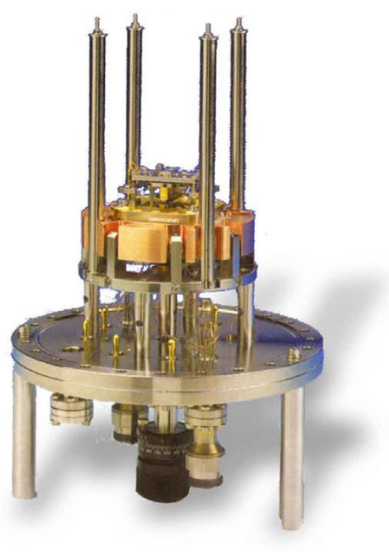


Figure 3. Photograph of the Truly Variable-Temperature Scanning Tunneling Microscope, complete with spring suspension and eddy current damping on a conflat flange. (courtesy of Leiden Probe Microscopy B.V.¹⁵)

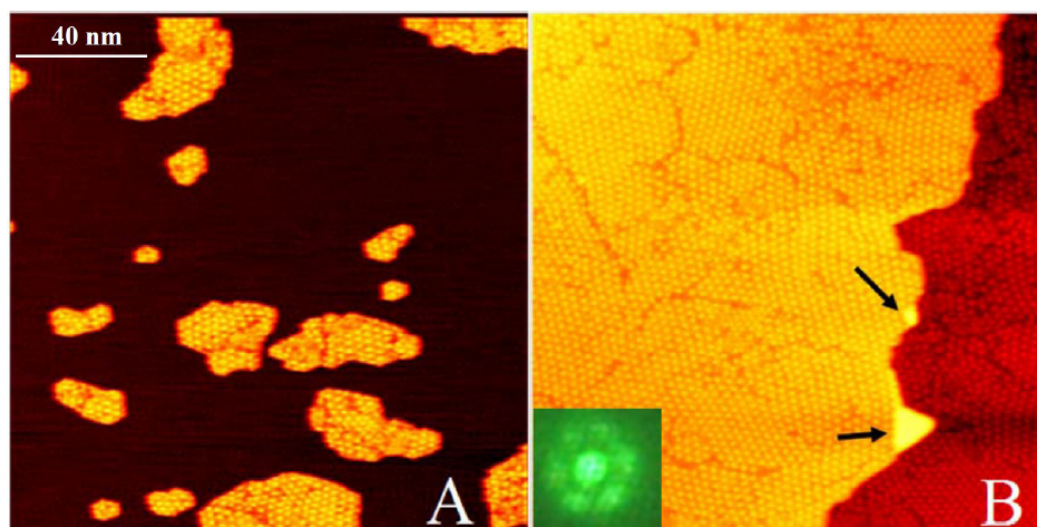


Figure 4. Figure 4. STM images of graphene formation on Rh(111), starting with a seeded surface. (A) The graphene-seeded Rh surface, obtained by annealing the rhodium surface to 975 K, after exposing it to ethylene at room temperature. (B) Graphene-covered surface, after further ethylene deposition at 975K. Notice the two Rh double-layer defects, indicated by the arrows. The inset in (B) shows the superstructure spots around a first-order LEED spot of the Rh substrate. Both STM images have a size of 160 nm × 160 nm. (from ref. 17)

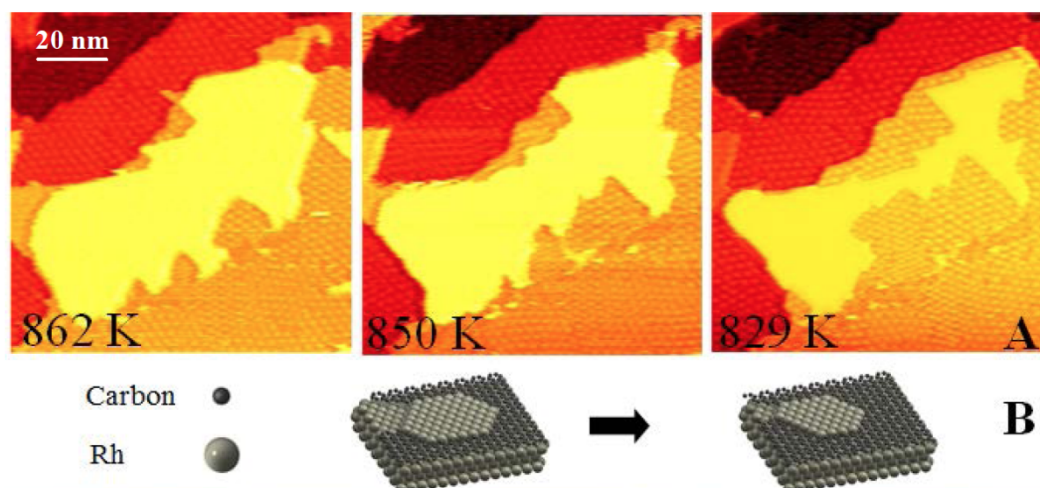


Figure 5. Graphene formation by segregation of dissolved carbon. (A) STM images of the same area during the cooling down of Rh(111), partly covered by graphene, after the room-temperature seeding procedure and ethylene exposure at 977K. The central rhodium terrace is at the same level as the surrounding graphene, implying that rhodium atoms are diffusing out of this area as the graphene grows. Image size: 100 nm \times 100 nm. (B) Ball model illustrating the growth of graphene through segregated carbon and the corresponding reduction of Rh area. (after ref. 17)

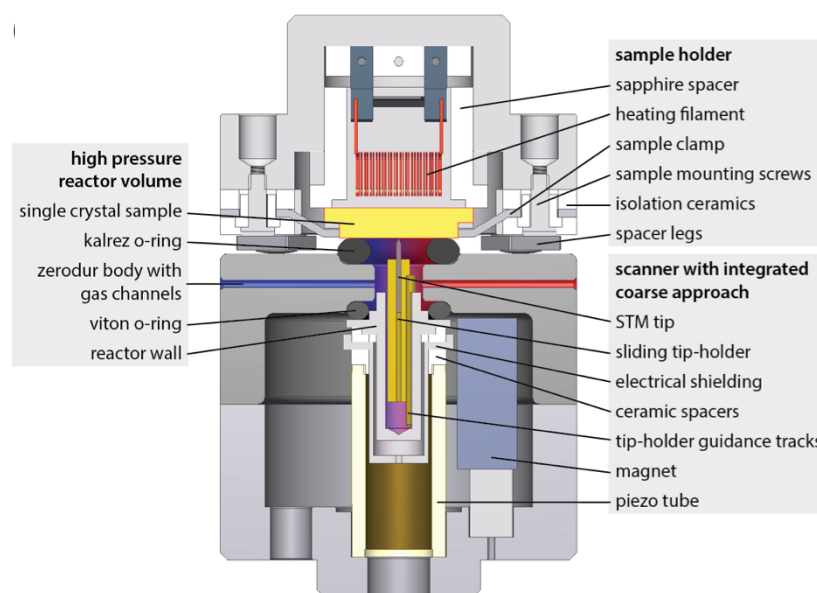


Figure 6. Schematic cross section of the central components of the ReactorSTM. The (yellow) sample is held in a sample holder (top part) with a heater, thermocouple and electrical connections. Here, the sample is placed on top of the STM scanner part of the system. In this position, it forms the ‘lid’ of the 500 μ l reactor. The reactor body is made of Zerodur glass. The reactants enter via a capillary from the left (blue) and the reacted gas mixture leaves the reactor through a capillary on the right (red), where it is connected to a separate Mass

Spectrometry system. The small reactor is sealed off against the sample surface via a Kalrez seal and against the top of the piezo element with a Viton seal. The piezo element itself remains in ultrahigh vacuum. (from ref. 20)

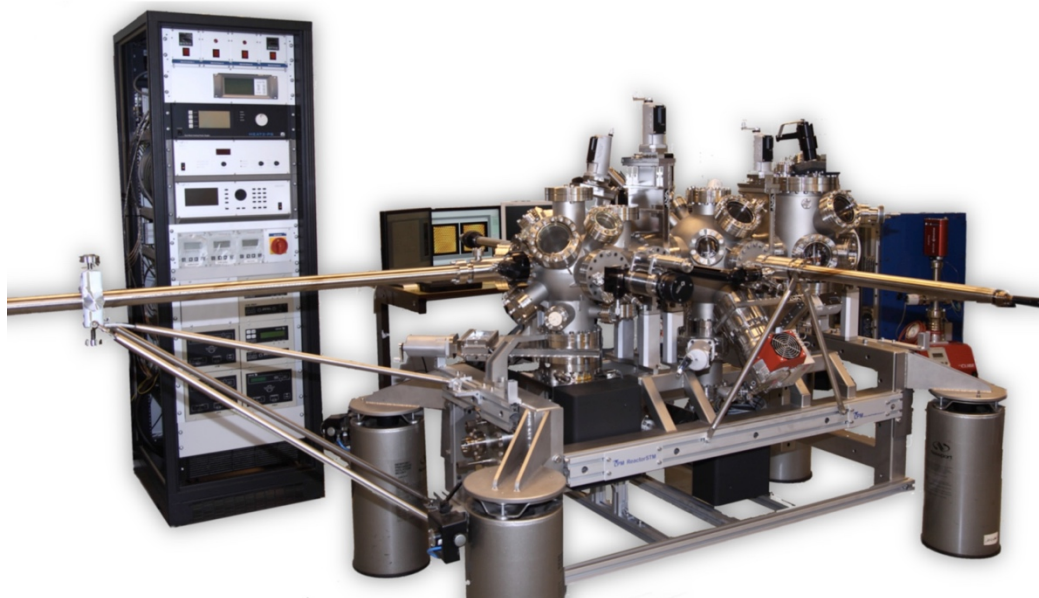


Figure 7. Photograph of the complete ReactorSTM system. (courtesy of Leiden Probe Microscopy B.V.¹⁵)

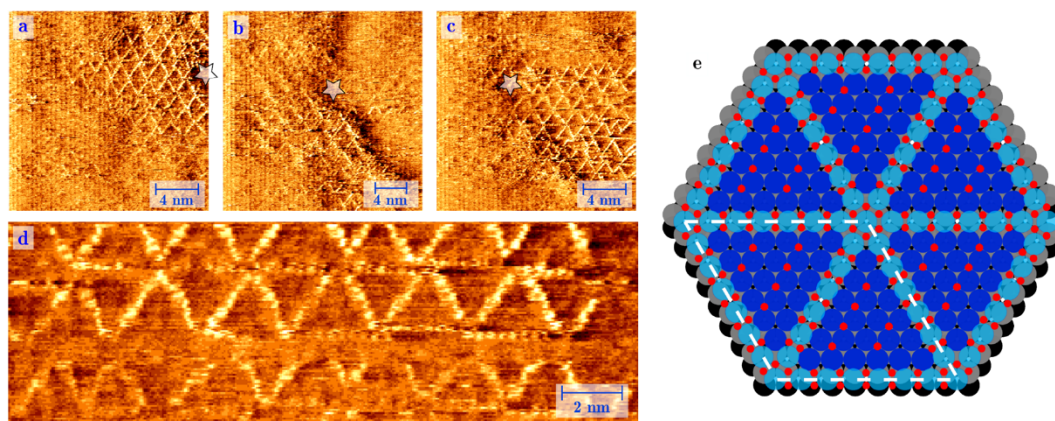


Figure 8. STM observations of Pt(111) in 1 bar O₂ at 529 K. A spoked-wheel motif with embedded PtO₂ rows can be recognized, with a variety of structural defects. Panels (a)-(c) show larger domains of this structure; the star serves as a reference point and indicates slow thermal drift. The enlarged detail in panel (d) shows the atomic resolution within the spokes. Panel (e) is the ball model with the oxidized Pt atoms in light blue, the O atoms in red and the regular Pt surface atoms in dark blue (layer 1), grey (layer 2) and black (layer 3). (from ref. 21)

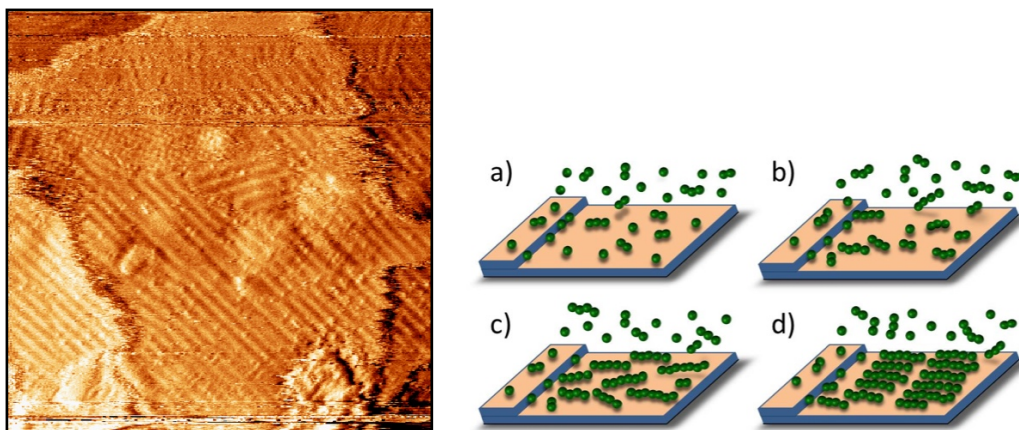


Figure 9. STM image of the Co(0001) surface, 40 min after the start of its exposure to 4 bar of an 1:2:2 mixture of CO, H₂ and Ar at a temperature of 483 K. The schematic pictures on the right illustrate how the overlayer forms as rows of well-organized hydrocarbon molecules. (after ref. 27)

Author biographies

Prof.dr. Joost W.M. Frenken, Advanced Research Center for Nanolithography,
P.O. Box 93019, 1090 BA Amsterdam, the Netherlands, +31-20-8517100,
frenken@arcnl.nl



Prof. Joost W.M. Frenken is the Director of the Advanced Research Center for Nanolithography in Amsterdam and a Professor in Physics at the University of Amsterdam and the VU University Amsterdam. His interests are on dynamic phenomena at surfaces and interfaces, including phase transitions, diffusion, nucleation and growth, catalysis and friction. For this, Frenken has developed several dedicated scanning probe and x-ray scattering instruments. Frenken is a member of the Netherlands Academy of Arts and Sciences (KNAW) and co-founder of two companies.

Dr. Irene M.N. Groot, Leiden Institute of Chemistry, P.O. Box 9502, 2300 RA
Leiden, the Netherlands, +31-71-5277361, i.m.n.groot@lic.leidenuniv.nl



Dr. Irene M.N. Groot is assistant professor in operando research in heterogeneous catalysis at the Leiden Institute of Chemistry. She is interested in unraveling the structure-performance relationship of model catalysts at the atomic scale under industrial conditions using advanced microscopy techniques. In her group she investigates CO oxidation, NO reduction and oxidation, hydrodesulfurization, Fischer-Tropsch synthesis, and methanol steam reforming using operando scanning tunneling microscopy, surface X-ray diffraction, and optical microscopy. This work is performed in close collaboration with industrial partners.